Available online at www.sciencedirect.com
SCIENCE DIRECT®
Journal of Magnetic Resonance 161 (2003) 138–147
JMR Journal of Magnetic Resonance
www.elsevier.com/locate/jmr

Predictions of pulsed field gradient NMR echo-decays for molecules diffusing in various restrictive geometries. Simulations of diffusion propagators based on a finite element method

Håkan Hagslätt,[a,*] Bengt Jönsson,[b] Magnus Nydén,[a] and Olle Söderman[c]

[a] *Department of Applied Surface Chemistry, Chalmers University of Technology, SE-412 96 Göteborg, Sweden*
[b] *Biophysical Chemistry, Center for Chemistry and Chemical Engineering, P.O. Box 124, SE-221 00 Lund, Sweden*
[c] *Physical Chemistry 1, Center for Chemistry and Chemical Engineering, P.O. Box 124, SE-221 00 Lund, Sweden*

Received 27 June 2002; revised 11 October 2002

Abstract

Pulsed field gradient NMR diffusometry is a promising tool for investigating structures of porous material through determinations of dynamic displacements of molecules in porous systems. A problem with this approach is the lack of closed analytical expressions for echo-decays in anything but idealized pore geometries. We present here an approach based on calculating the appropriate diffusion propagator by means of finite element calculations. The suggested method is quite general, and can be applied to arbitrary porous systems. The protocol for the calculations is outlined and we show results from some different cases: diffusion in confined geometries and in systems that are spatially inhomogeneous with respect to concentration.

Keywords: Propagator; Diffusion; Finite element method; Simulation; Pulsed field gradient NMR

1. Introduction

The application of pulsed field gradient (PFG) NMR for monitoring molecular displacements in inhomogeneous systems is an increasingly used experiment in chemistry, physics and medicine. Results from a PFG experiment performed on an inhomogeneous system may differ substantially from those from the same experiment performed on a homogenous system [1–3]. The presence of local heterogeneities leads to spatial variations in the equilibrium concentration and the values of the diffusion constants, and this is reflected in the appearance of the echo-decays. This is particularly evident in the "q-space" formalism, in which the echo-decays are presented as a function of the variable $q = \gamma g \delta / 2\pi$ [4,5]. q has units of inverse length and the presence of characteristic lengths in the investigated system may give rise to both minima and maxima in the echo-decays [4,6–9]. Thus the experiment conveys structural information by providing values of the mean square displacements of the molecules comprising the system.

The length-scale to which the experiment is sensitive, is related to the maximum gradient strength that a particular experimental set-up may generate. For a representative case, the experiment is tuned to length-scales in the μm regime, and thus is of particular interest to scientists working in colloidal systems [10]. In biological and physiological studies, such as for instance studies of erythrocytes, the spinal cord and the human brain, relevant structural length scales are well tuned to the application of PFG based NMR methods [6,11,12]. For systems that are homogeneous on this length-scale, the NMR experiment may generate the effective diffusion coefficient, the value of which is dependent on all local heterogeneities of the system (e.g., on the nm-scale).

One of the problems of the PFG approach is to develop a theoretical framework with which the experimental results may be interpreted, so as to extract the relevant information. It turns out that for anything but

* Corresponding author. Fax: +46-31-160062.
E-mail address: hakan.hagslatt@surfchem.chalmers.se (H. Hagslätt).

1090-7807/03/$ - see front matter © 2003 Elsevier Science (USA). All rights reserved.
doi:10.1016/S1090-7807(02)00039-3

very simple geometries of barriers (such as rectangular and cylindrical barriers) no exact solutions exist and one has to resort to numerical methods in order to interpret the data [1]. Such approaches rely on either Brownian dynamic simulations or numerical solutions of the relevant differential equations [13–16]. The necessary calculations are time-consuming and difficult if possible at all to apply to complex geometries. One promising approach to treat complex geometries relies on the use of artificial neural networks [17,18].

In this work, which is the first in a series of papers, we present an approach that is based on the use of finite element calculations in order to generate the appropriate propagator $P(z_0|z,\Delta)$ [9], which is then used to calculate the echo-decay from the master equation

$$E_\Delta(q) = \int \rho(z_0) \int P(z_0|z,\Delta)\, e^{i2\pi q\cdot(z-z_0)}\, dz\, dz_0, \qquad (1)$$

where $\rho(z_0)$ is the initial density of the spin bearing molecules and the propagator $P(z_0|z,\Delta)$ is the probability density that a molecule originally at z_0 has moved to z after a time Δ. It should be remarked that the use of Eq. (1) assumes that the gradient pulses are infinitely narrow (the short-gradient pulse (SGP) approximation). A discussion of the validity of Eq. (1) can be found in [15,19,20].

The approach can be applied to an arbitrary geometry. In fact, one application of the method is to calculate the echo-attenuation from a "real-space" image, obtained for instance by means of the confocal laser microscopy technique.

In this paper we outline the method, and apply it to some geometries that are chosen in order to demonstrate the validity of the method and its applicability to systems of any level of complexity. Hence, we calculate echo-decays on basis of simulated propagators for three systems for which exact solutions: free diffusion, spins confined between parallel reflective barriers and spins enclosed in a circular region. The simulated results and analytical solutions are then compared. Subsequently, we present calculations for systems for which exact solutions are not available. In one, we treat a lamellar system composed of alternating regions of equal length but different concentrations of the diffusing molecule. Similar problems have been treated in references [18,21,22]. Another system is a hexagonal lattice of circular regions in which the concentration is different from that in the surrounding continuous medium. Finally, a model of a cellular system of still higher complexity is studied.

2. Simulation of diffusion propagators by means of a finite element method

In this work, we present a methodology to numerically simulate the propagator in highly complex systems by means of a finite element method. Briefly, the numerical protocol involves to define the unit cell and the dimensions of the space for which simulations should be performed, chose an equation that appropriately describes the composition and driving forces for molecular displacement and define relevant coefficients and boundary conditions, and subsequently to perform the simulation of the propagator as a function of z_0, z and Δ. In the examples given in the following section, the studied systems are assumed to be in chemical equilibrium, and the local equilibrium concentrations and local diffusion coefficients are assumed to be time independent. It is assumed that the PFG experiment itself does not affect the sample in any respect except for magnetically labeling the positions of the studied molecules at certain times. A detailed description of the numerical procedure is given in the following 8 subsections.

2.1. The dimension of the simulation box is specified

The smallest representative part of the studied system is chosen as a unit cell in the numerical simulation. The starting position of the studied molecules, z_0, is always inside this cell. Copies of the unit cell are placed in the z-direction on both sides of the original unit cell, as outlined for a 2-D box in Fig. 1. The central unit cell and the surrounding copies form a simulation box in which the diffusion of the labeled molecules is determined.

The number of cells that are needed on both sides of the original unit cell, depends on the maximum time, Δt_{max}, the system will be followed in the simulation. The total length on each side of the original unit cell, Δz_{max}, is chosen to be large enough to prevent unphysical effects from the outer boundary of the simulated system. The minimum value of Δz_{max} can be estimated from the concentration profile of a plane source, as given by Eq. (2),

$$c(z) = \frac{A}{\sqrt{t}} \cdot \exp\left(-\frac{z^2}{4D_{eff}\cdot t}\right) \qquad (2)$$

where D_{eff} is the effective diffusion coefficient in the z-direction over a unit cell and A is a constant. The value

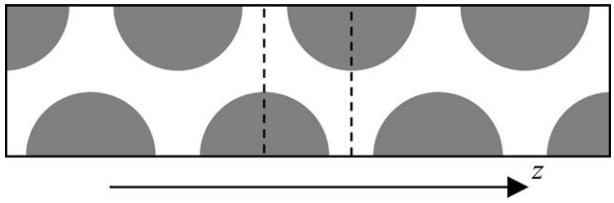

Fig. 1. A schematic representation of a simulation box. The area between the dashed lines constitutes the unit cell, i.e., the smallest representative part of the system in terms of diffusion in the z-direction. The central unit cell is surrounded on both sides in the z-direction by a number of copies of the unit cell, until the desired value of Δz_{max} is reached. Note that every second cell is a mirror image of the central unit cell in this case.

of $\Delta z_{\max}$ can be estimated from Eq. (2) if the maximum allowed concentration ratio $c(\Delta z_{\max})/c(0)$ at the time $\Delta t_{\max}$ is specified. For example, if the ratio is 0.001, the equation for $\Delta z_{\max}$ becomes

$$\Delta z_{\max} = \sqrt{\ln(10) \cdot 3 \cdot 4 \cdot D_{\text{eff}} \cdot \Delta t_{\max}} \leqslant 4 \cdot \sqrt{2 \cdot D_{\text{eff}} \cdot \Delta t_{\max}}. \quad (3)$$

2.2. The boundary conditions of the simulation box are specified

All external boundaries of the simulation box are treated as perfectly reflecting. For the boundaries in the x- and y-directions this is due to the symmetry of the simulation box. In the z-direction, only a negligible amount of the diffusing compound reaches the external boundaries, as described above, and the choice of boundary conditions is therefore of minor importance. Since the choice of reflecting boundary conditions is a convenient choice, we have used it throughout.

2.3. Chose an equation to describe the molecular transport in the studied system

To appropriately model the transport of molecules in a system where the local thermodynamic properties as well as the transport properties of the studied molecules differs between different regions of the system is a difficult task, since this requires a detailed knowledge of the chemical potential of the studied molecule in all parts of the system. On the other hand, to model the transport of NMR-labeled molecules in a system that is in equilibrium (except for the fact that some molecules have been labeled), is easier since the concentration of labeled plus unlabeled molecules (c_{eq}) is known in all parts of the system in this case.

For such a case, it is more convenient to use the molar ratio of labeled molecules, $X(x,y,z,t)$, than the concentration of labeled molecules, $c_{\text{labeled}}(x,y,z,t)$.

$$c_{\text{labeled}}(x,y,z,t) = c_{\text{eq}}(x,y,z) \cdot X(x,y,z,t). \quad (4)$$

The flux of labeled molecules, J_{labeled}, can be obtained from the general form of Fick's first law [23] as given in Eq. (5).

$$J_{\text{labeled}}(x,y,z,t) = -\frac{D(x,y,z)}{RT} \cdot c_{\text{labeled}}(x,y,z,t) \cdot \nabla \mu_{\text{labeled}}(x,y,z,t), \quad (5)$$

where $\nabla \mu_{\text{labeled}}(x,y,z,t)$ is the gradient in the chemical potential of the labeled molecules, $D(x,y,z)$ the local diffusion constant, R the gas constant and T the temperature. Since the system is in equilibrium, except for the fact that some molecules are labeled, the gradient of the chemical potential of the labeled molecules can be written as

$$\nabla \mu_{\text{labeled}} = \nabla(\mu_{\text{eq}} + RT \cdot \ln X) = \frac{RT}{X} \cdot \nabla X. \quad (6)$$

If Eq. (6) is used in Eq. (5), the flux equation becomes

$$J_{\text{labeled}}(x,y,z,t) = -D(x,y,z) \cdot c_{\text{eq}}(x,y,z) \cdot \nabla X(x,y,z,t). \quad (7)$$

Finally, a general form of the diffusion equation can be obtained by combining Eqs. (4) and (5), and the relation between the flux and the change of concentration with respect to time.

$$c_{\text{eq}}(x,y,z) \cdot \frac{\partial(X(x,y,z,t))}{\partial t} = \nabla \cdot \big(D(x,y,z) \cdot c_{\text{eq}}(x,y,z) \cdot \nabla X(x,y,z,t)\big). \quad (8)$$

This equation was used to describe the molecular transport in the simulations.

The two main reasons for introducing the mole fraction, X, together with Eq. (8) instead of using the normal diffusion equation are:

(a) X is a continuous function in all parts of the simulation box and when Eq. (8) is solved by a finite element method, no internal boundary conditions between different regions have to be specified. All information about the transport properties of the studied system is given in the equilibrium concentration, $c_{\text{eq}}(x,y,z)$, and the local diffusion coefficient, $D(x,y,z)$.

(b) Eq. (8) can be used for systems with all types of intrinsic concentration and diffusion constant profiles.

Finally, we note that no permeabilities across internal boundaries need to be introduced. The diffusion equation is defined solely by local concentrations and diffusivities.

2.4. Reject regions where the equilibrium concentration is zero

Regions where the equilibrium concentration is zero are excluded from the simulation box and reflecting boundary conditions are used to delimit these regions.

2.5. Select a numerical program to solve the generalized diffusion equation

Different numerical programs can be used to solve Eq. (8). We have used FEMLAB [24], which is a program based on the finite element method and that operates together with MATLAB [25]. The simulation box is divided into a mesh in this program, see Fig. 2, and the mole ratio of marked molecules, X, is calculated at each mesh point by a finite element method.

In the work presented here, we have, for reasons of simplicity, performed calculations in 2-dimensions. However, the strategy to follow is analogous for simulations in 3-dimensions, although these are of course computationally more demanding.

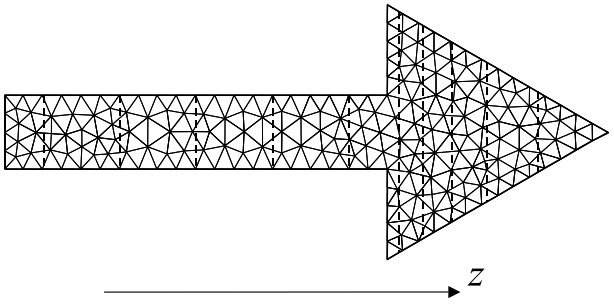

Fig. 2. The simulation box in the FEMLAB program is automatically divided into a mesh. The number of mesh points can be increased in the simulation until no effects of the mesh size is observed. Displayed are also 10 concentration weighted starting positions in a unit cell (dashed lines).

2.6. A number of different starting positions, z_0-values, are specified

To be able to determine the mean propagator for the system of interest, the propagators for a number, n, of representative starting positions inside the central unit cell, must be calculated. Two different patterns of starting positions have been used:

(a) Equally spaced starting positions

$$z_{0,i} = z_{0,\min} + (i-0.5)\cdot\frac{z_{0,\max}-z_{0,\min}}{n} \quad \text{for } 1 \leqslant i \leqslant n. \tag{9}$$

Starting positions chosen according to Eq. (9) have been used in most of the presented simulations.

(b) Concentration weighted starting positions.

The $z_{0,i}$ values are obtained from the following equation.

$$\int_{z_{0,\min}}^{z_{0,i}} \int\int_{\text{all}\,x,y} c_{\text{eq}}(x,y,z)\,\mathrm{d}x\,\mathrm{d}y\,\mathrm{d}z = \frac{(i-0.5)}{n} \cdot \int\int\int_{\text{unit cell}} c_{\text{eq}}(x,y,z)\,\mathrm{d}x\,\mathrm{d}y\,\mathrm{d}z \quad \text{for } 1 \leqslant i \leqslant n. \tag{10}$$

This choice of starting positions is in most cases optimal, especially in systems where the number of molecules is much higher in one part of the unit cell than in the rest. As an example, we show in Fig. 2 an arrow-shaped geometry, which serves the purpose of illustrating the principle. Ten starting positions with equal number of molecules between two adjacent positions are shown in Fig. 2.

2.7. Determine, at selected time intervals, the diffusion propagator for each of the selected starting positions

In an ideal simulation of the propagator $P(z_0|z,\Delta)$, the time evolution of a very narrow concentration profile, centered at z_0, is followed. However, since it is very time consuming to numerically determine the initial time evolution of a very narrow concentration profile, we have omitted a detailed description of the initial diffusion process. Instead, we start the simulation at a time $\Delta t_{\min}$ and follow the evolution of the mole fraction, X, from that time. The X-profile in a bulk solution at time $\Delta t_{\min}$, is a Gaussian error curve with a standard deviation $\sqrt{2\cdot D_{\text{eff}}(z_0)\cdot\Delta t_{\min}}$, see Eq. (11)

$$X(z,\Delta t_{\min}) = \frac{1}{\sqrt{4\pi\cdot D_{\text{eff}}(z_0)\cdot\Delta t_{\min}}} \cdot \exp\left(-\frac{(z-z_0)^2}{4D_{\text{eff}}(z_0)\cdot\Delta t_{\min}}\right). \tag{11}$$

In or near a region where the equilibrium concentration is changing as a function of z, the profile will be more complicated and can in general not be written as an analytic function. However, since no simple general description of the $X(z,\Delta t_{\min})$ profile can be obtained for most systems, we have used a discontinuous mole fraction profile according to Eqs. (12a) and (12b)

$$X(z,\Delta t_{\min}) = \frac{1}{2\Delta z_{\min}} \quad \text{if } |z-z_0| \leqslant \Delta z_{\min} \tag{12a}$$

else

$$X(z,\Delta t_{\min}) = 0, \tag{12b}$$

where $\Delta z_{\min}$ is chosen to give the same mean square displacement,

$$\langle z^2\rangle = \frac{\int X(z)\cdot z^2\,\mathrm{d}z}{\int X(z)\,\mathrm{d}z} \tag{13}$$

in the discontinuous profile as in the Gaussian profile, i.e., $2\cdot D_{\text{eff}}(z_0)\cdot\Delta t_{\min}$. This gives

$$\Delta z_{\min} = \sqrt{6\cdot D_{\text{eff}}(z_0)\cdot\Delta t_{\min}} \tag{14}$$

The neglect of a detailed description of the mole ratio profile at $\Delta t_{\min}$ introduces an error in the simulations. However, this error is only important at times near $\Delta t_{\min}$ and can in most cases be neglected at longer time intervals. It is difficult to give a general estimation of the $\Delta z_{\min}$ value needed to obtain a specific time resolution in a simulation. A successive reduction of $\Delta z_{\min}$, until the effect of the simplified starting configuration is acceptable, is in most cases the only way to specify a necessary $\Delta z_{\min}$ value. Eq. (14) predicts that if water is studied, for which $D = 2\times10^{-9}$ m^2 s^{-1} at 25 °C, and if the time $\Delta t_{\min}$ is 1 ms (this time resolution is in most cases accurate enough to simulate a PFG echo-decay experiment), the distance $\Delta z_{\min}$ is 3.5 μm.

The propagator for molecules starting at position z_0 can for a selected time, Δ, be calculated from Eq. (15)

$$P(z_0|z,\Delta) = \frac{\int\int_{\text{all}\,x,y} c_{\text{eq}}(x,y,z)\cdot X(x,y,z,\Delta)\,\mathrm{d}x\,\mathrm{d}y}{\int_{z_0-\Delta z_{\min}}^{z_0+\Delta z_{\min}}\int\int_{\text{all}\,x,y} c_{\text{eq}}(x,y,z)\cdot X(x,y,z,\Delta t_{\min})\,\mathrm{d}x\,\mathrm{d}y\,\mathrm{d}z}, \tag{15}$$

where the X-profile started as the profile given by Eqs. (12a) and (12b) at $\Delta t_{\min}$. Since $X(x,y,z,\Delta)$ is always proportional to the $X(x,y,z,\Delta t_{\min})$-value it is clear from Eq. (15) that the starting value of X at $\Delta t_{\min}$, $X(x,y,z,\Delta t_{\min})$, will not influence the form of the propagator. This means that an arbitrary, but constant, $X(x,y,z,\Delta t_{\min})$-value for $|z-z_0| \leqslant \Delta z_{\min}$ can be used instead of the value proposed by Eq. (12a).

2.8. The effective diffusion propagator for the studied system is determined at the selected time intervals

Instead of saving, for further evaluation, the propagators for each of the starting positions the effective propagator, averaged over all relevant starting positions and weighted by the initial probability density of the studied compound, is evaluated

$$\langle P(z-z_0|\Delta)\rangle = \frac{\int\int\int_{\text{unit cell}} c_{\text{eq}} \cdot P(z_0|(z_0+(z-z_0)),\Delta)\,\mathrm{d}x_0\,\mathrm{d}y_0\,\mathrm{d}z_0}{\int\int\int_{\text{unit cell}} c_{\text{eq}}\,\mathrm{d}V}. \tag{16}$$

The propagator for each starting position, z_0, is weighted by the number of molecules in the starting band $(z_0-\Delta z_{\min}) < z < (z_0+\Delta z_{\min})$ and then written as a function of $(z-z_0)$. The effective propagator for the studied system is subsequently obtained from the sum of all weighted propagators divided by the total number of molecules in all starting bands.

$$\langle P(z-z_0|\Delta)\rangle \approx \frac{\sum_{i=1}^{n} n_i \cdot P_i(z_0|(z_0+(z-z_0)),\Delta)}{\sum_{i=1}^{n} n_i} \tag{17}$$

The results contain errors that are associated with the finite number of starting positions. However, this error is reduced when the number of starting positions increases and a Richardsson extrapolation scheme can be used to further decrease the errors introduced by the finite number of starting positions [26].

3. Results and discussion

In this section we present the results of some simulations performed using the approach described above. We start by presenting results for three cases were analytical solutions exist, in order to establish that the exact results are correctly reproduced if the simulations are performed according to the above described methodology, and to discuss the errors that may be introduced. We then perform simulations for a few systems that are inhomogeneous with respect to molecular compositions, and where no analytical solutions are available. In all cases, it is assumed that the PFG experiment itself does not affect the sample in any respect except for magnetically labeling of the positions of the studied molecules at certain times. Moreover, the echo attenuations are evaluated according to Eq. (18) on the assumption that infinitely narrow gradient pulses are applied.

$$E_{\Delta}(q) = \int < P(z-z_0|\Delta) > \cdot \mathrm{e}^{\mathrm{i}2\pi q\cdot(z-z_0)} d(z-z_0). \tag{18}$$

3.1. Free diffusion

For a homogenous system without boundaries for diffusion, the propagator $P(z_0|z,\Delta)$ is a Gaussian [1] and Eq. (1) then predicts the following echo-decay

$$E_{\Delta}(q) = \mathrm{e}^{-4\pi^2 q^2 \Delta D} \tag{19}$$

The echo-decays resulting from the simulation of the diffusion of molecules starting in the center of an 800 μm wide simulation box are presented in Fig. 3 at three different q-values. For each q-value, Δ has been varied. The agreement between the numerically generated data and the exact solution, given by Eq. (19), is quantitative in a Δ-range of about 0.001–3 s. A small difference can be observed at the shortest times in the $q = 3\times10^5\,\mathrm{m}^{-1}$ graph, and this is due to the simplified start concentration profile at $\Delta t_{\min} = 1\times10^{-4}$ s (corresponding to $\Delta z_{\min} = 1\,\mu\mathrm{m}$). The difference at the longest times is due to reflections in the z-boundaries of the simulation box. As shown in the figure for $q = 10^3\,\mathrm{m}^{-1}$, the time when this effect starts to be important is at $t \approx 6\times10^6/q^2 = 6$ s. This time can be compared with the $\Delta t_{\max}$ value from Eq. (3), $\Delta t_{\max} = 2.5$ s.

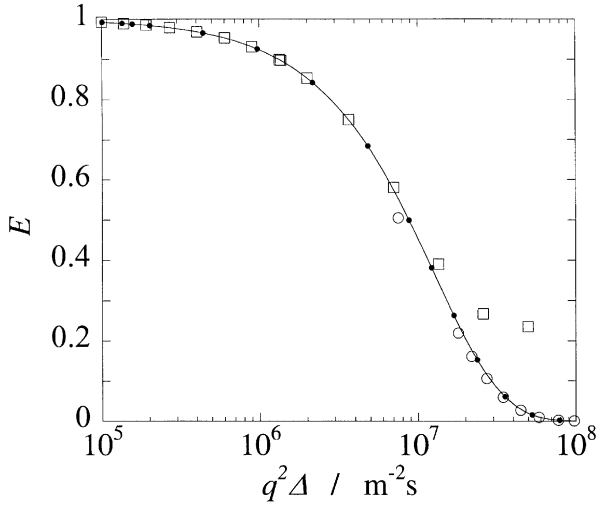

Fig. 3. The simulated (symbols) and exact (solid line) echo-decays for a homogeneous system as a function of $q^2\Delta$ for three different q values (with the maximum Δ-value given in parenthesis), □, $1\times10^3\,\mathrm{m}^{-1}$ (100 s); ●, $9.4\times10^3\,\mathrm{m}^{-1}$ (1.13 s); ○, $3\times10^5\,\mathrm{m}^{-1}$ (1.11 ms). The diffusion coefficient of the simulated molecules is $D = 2\times10^{-9}\,\mathrm{m}^2\,\mathrm{s}^{-1}$, $\Delta z_{\max} = 0.4$ mm, and $\Delta t_{\min} = 10^{-4}$ s.

3.2. Diffusion in inhomogeneous systems

In the following sections, we turn our attention to systems where the propagation of the simulated molecules is followed from several starting positions. The numerical errors of the simulated echo attenuations can be made very small, by using an appropriate number of starting positions, mesh points, etc. In the data presented below, the absolute errors are of the order of 5×10^{-4} or less in each point, while the relative errors are smaller than about 0.5% in each point. In order to reach these error levels, between 30 and 100 starting positions and $\Delta t_{\min} \sim 10^{-5}$ s have typically been used.

3.3. Restricted diffusion between reflecting planes

We have studied an inhomogeneous system in which the spins are confined to the region between two parallel reflecting planes, with the gradient applied parallel to the plane normal. Exact solutions for the echo-decays from such systems exist within the short-gradient pulse limit [21]. We have simulated echo-decays for molecules with a diffusion coefficient of $D = 2 \times 10^{-9}\,\mathrm{m^2\,s^{-1}}$ and a distance between the planes of $a = 20\,\mu\mathrm{m}$. Since the walls of the unit cell are impermeable, the simulation box is the same as the unit cell. The data are presented in Fig. 4 together with data from the analytical solution.

It should also be mentioned that the observed minima are due to phase cancellations that often occur when studying molecules that exhibit restricted diffusion in well-defined pores. For a rectangular geometry, minima occur for $q = n/a$, where n is a positive integer.

3.4. Restricted diffusion in a cylinder

We now turn to diffusion perpendicular to the symmetry axis of molecules confined to a cylinder with impermeable walls, which is another case where the simulation box is the same as the unit cell. As before we have chosen to investigate molecules with $D = 2 \times 10^{-9}\,\mathrm{m^2\,s^{-1}}$, and the radius R of the cylinder was set equal to 10 μm. The numerically evaluated echo attenuation and the analytical solution are presented in Fig. 5.

3.5. Diffusion in a lamellar system

As is evident from the examples presented above we are able to correctly predict echo-decays for both free diffusion and for diffusion restricted by the presence of impermeable barriers. We now turn to systems in which the concentration of molecules shows a spatial variation in the sample. This is a common situation, for instance in many biological systems, where the structure on a cellular level constitutes one example [6,18]. We consider a system, outlined in the insert in Fig. 6, of alternating slabs, each with the same thickness of 20 μm and each with the same diffusion coefficient ($D = 2 \times 10^{-9}\,\mathrm{m^2\,s^{-1}}$) but with a factor of 10 difference in equilibrium concentrations between two adjacent slabs.

In the long-time limit, the effective diffusion coefficient for such a system is given by

$$D_{\mathrm{eff}} = \left(\frac{1}{C_1\Phi_1 + C_2\Phi_2}\right) \cdot \left(\frac{\Phi_1}{C_1 D_1} + \frac{\Phi_2}{C_2 D_2}\right)^{-1}, \qquad (20)$$

where C_i, D_i, and Φ_i $(i = 1, 2)$ are the equilibrium concentrations, diffusion coefficients and volume fractions of the two regions, respectively. Using the values given

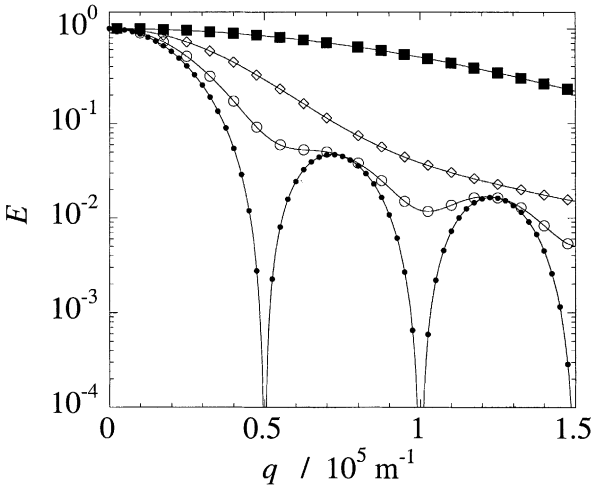

Fig. 4. The simulated (symbols) and exact (solid lines) echo-decays from the molecules between two reflecting walls as a function of q for four different Δ-values, ■, 1 ms; ◇, 10 ms; ○, 32 ms; ●, 1 s. The distance between the reflecting planes is 20 μm and the diffusion coefficient of the simulated molecules is $D = 2 \times 10^{-9}\,\mathrm{m^2\,s^{-1}}$.

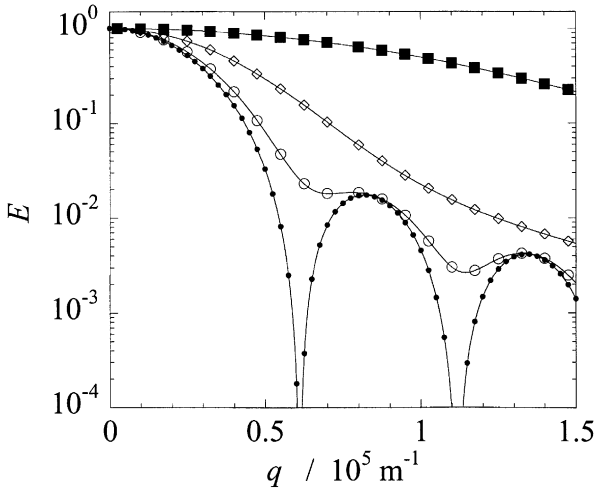

Fig. 5. The simulated (symbols) and exact (solid lines) echo-decays resulting from the radial diffusion of molecules confined in a cylinder with reflecting walls after diffusion times of ■, 1 ms; ◇, 10 ms; ○, 32 ms; ●, 1 s. The radius of the cylinder is 10 μm and the diffusion coefficient of the simulated molecules is $D = 2 \times 10^{-9}\,\mathrm{m^2\,s^{-1}}$.

above, one obtains $D_{\text{eff}} = 0.661 \times 10^{-9}\,\text{m}^2\,\text{s}^{-1}$, and hence the size of the simulation box of $\Delta z_{\max} = 0.51 \times 10^{-3}\ m$ used in the simulation, corresponds to $\Delta t_{\max} = 12\,\text{s}$, according to Eq. (3). The subsequently calculated echo-decays for some different diffusion times are displayed in Figs. 6 and 7.

For this system, no exact time-resolved solution is available, but the effective diffusion coefficient is available, as described above. An estimation of the long-time errors of the simulation can therefore be obtained, since the effective diffusion coefficient is related to the mean squared displacements of the molecules through

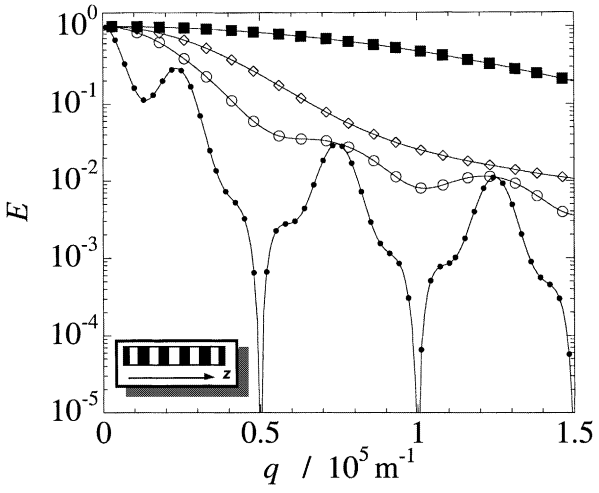

Fig. 6. The simulated echo-decay from molecules in a lamellar system shown in the insert after diffusion times of ■, 1 ms; ◇, 10 ms; ○, 32 ms; ●, 1 s. The symbols represent a limited selection of the total set of 150 data points per solid line. The thickness of each region is 20 μm and the ratio between the equilibrium concentrations of two adjacent regions is 10. The diffusion coefficient of the simulated molecules is in both regions $D = 2 \times 10^{-9}\,\text{m}^2\,\text{s}^{-1}$ and $\Delta z_{\max} = 0.51$ mm.

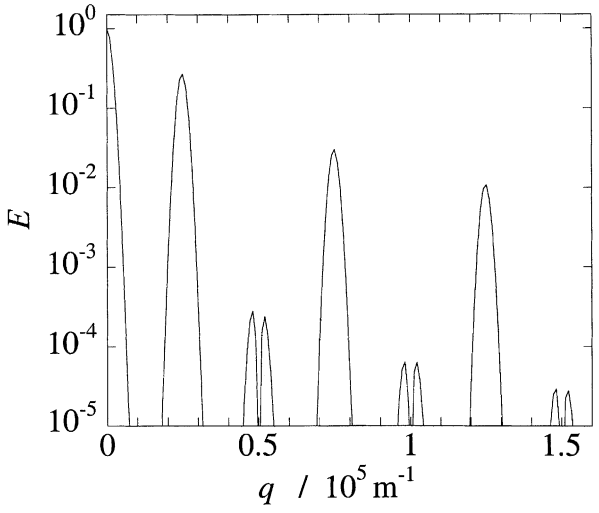

Fig. 7. The simulated echo-decay for the same system as in Fig. 6, after a diffusion time of 10 s.

$$D_{\text{eff}} = \frac{\langle z^2 \rangle_{\text{long-time}}}{2\Delta}. \tag{21}$$

The quantity $\langle z^2 \rangle_{\text{long-time}}$ as obtained from the echo-decays at long diffusion time (10 s) and low q-values [4] results in $D_{\text{eff}} = 0.661 \times 10^{-9}\,\text{m}^2\,\text{s}^{-1}$, in good agreement with the analytical result.

Furthermore, we can make use of the observed peaks and minima of Fig. 7 in order to investigate the reliability of the performed simulation. Peaks are found at values of q which are centered around $q = n_c\ 2.5 \times 10^4\,\text{m}^{-1}$, where n_c are positive integers. For even values of n_c, the peaks are split and of considerably lower intensity. Supported by the data presented in Fig. 6, especially the graph representing a diffusion time of 1 s, this result indicates the presence of nodes located at $q = n_n\ 5 \times 10^4\,\text{m}^{-1}$, where n_n are positive integers.

These observations can be rationalized by the physics of the lamellar system and its characteristic distances as follows. First, we have the thickness of each slab, which corresponds to the distances between the reflective boundaries as described above. We would hence expect to observe minima due to phase cancellation at values of $q = n\ 5 \times 10^4\,\text{m}^{-1}$, similarly to the results presented in Fig. 4. In addition, because of the regular underlying lattice, phase coherences may be observed (see the book by Callaghan [1] for a lucid account of these phenomena). In the present system we expect to observe such coherences at multiples of 40 μm (the nearest distance between the centers of two concentration rich slabs), i.e. at q-values of $q = n\ 2.5 \times 10^4\,\text{m}^{-1}$. By a comparison with the simulated results, it can be concluded that all these expected features are present.

3.6. Echo-attenuation in an inhomogeneous system with hexagonal symmetry

Echo attenuations were evaluated for diffusion along the z-axis of a hexagonal system as given in Fig. 8, which is a 2-D representation of cylinders, hexagonally ordered in a solvent, which we take to be water. The distribution of the diffusing compound is 1:0.1 between the water and the cylinders and $D = 2 \times 10^{-9}\,\text{m}^2\,\text{s}^{-1}$ for both domains. Each phase constitutes half of the sample volume, the cylinder radius is 10 μm and hence the distance between the centers of two adjacent cylinders is $d \approx 27\,\mu\text{m}$.

The probability density profile for the diffusing compound of this system as a function of time and starting position have been evaluated numerically, with $\Delta z_{\max} = 0.41 \times 10^{-3}\,\text{m}$ used for the simulation box corresponding to $\Delta t_{\max} = 4\,\text{s}$, according to Eq. (3). The subsequently evaluated spin echo attenuation is given in Fig. 9.

Coherence peaks are noted for $q = n/(d/2)$, which corresponds to the distances between the centers of the

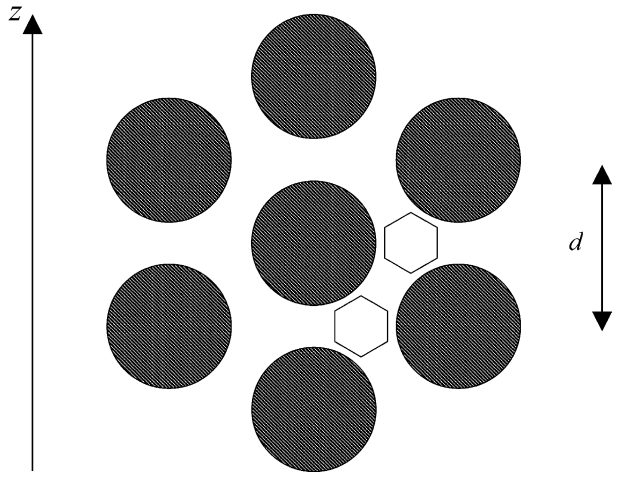

Fig. 8. A schematic representation of a system with cylindrical rods in a hexagonal lattice. The radius of a cylinder is 10 μm and the center–center distance (d between two adjacent cylinders is 27 μm. The distance in the z-direction between the centers of two neighboring "water-domains," as indicated by the two hexagons in the figure, is $d/2$.

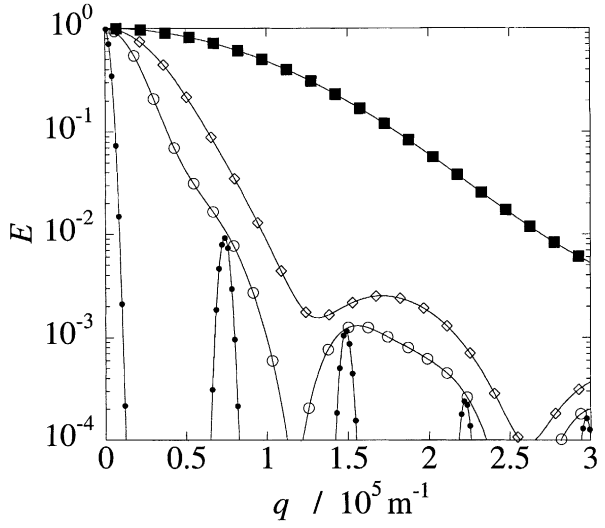

Fig. 9. The simulated echo-decays from the molecules in the hexagonal system shown in Fig. 8 at Δ-values of ■, 1 ms; ◇, 10 ms; ○, 32 ms; ●, 1 s. The symbols represent a limited selection of the total set of 500 data points per solid line. The equilibrium concentration of the studied molecules is 10 times lower inside a cylinder compared with the surrounding region. The diffusion coefficient of the simulated molecules is in both regions $D = 2 \times 10^{-9}\,\mathrm{m^2\,s^{-1}}$.

inter-particle water domains in the z-direction, as shown in Fig. 8.

3.7. Diffusion in more complex systems

The systems discussed above have rather simple geometric structures, but the presented simulation technique is not limited to this type of systems, since the finite element method that we have used is well adapted also to treat complex structures. An example of a more complex

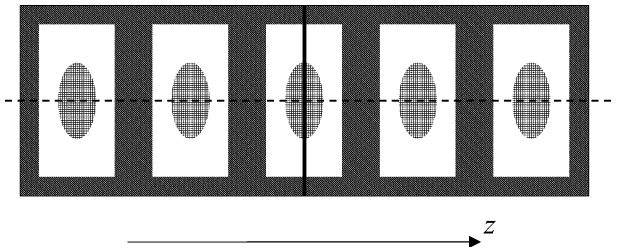

Fig. 10. Five-unit cells of a system where each unit cell is made up of a rectangular water domain of size $20 \times 40\,\mu\mathrm{m}^2$ (white), which is covered by a 5 μm thick wall (dark grey) where the equilibrium water concentration is reduced to 1/10, and contains an elliptic core (grid) with semi-axes 5 and 10 μm, respectively, in which the water equilibrium concentration is half of that of the water domain. The central, thin black rectangle indicates the starting pulse, and simulated propagators along the dashed line are given in Fig. 11.

structure is the system represented in Fig. 10. It is made up of a rectangular water domain, which contains an elliptic core. A wall surrounds each such domain. We have simulated the diffusion in this system using molecules for which the diffusion constant is $D = 2 \times 10^{-9}\,\mathrm{m^2\,s^{-1}}$ in all three regions, and the relative equilibrium concentrations of the studied molecules in the core, the pure water domain and the wall is 0.5:1:0.1. The probability density distribution in the z-direction along the center of the simulation box after propagation for 10^{-3}, 10^{-2}, and 0.3 s, for molecules that were located in a 0.2 μm thin band in the center of the central unit cell at $\Delta t_{\min}$ is given in Figs. 11a–c, together with the equilibrium state of the system in Fig. 11d. It should be noted that the concentration scales of the figure are arbitrary, and that the absolute concentrations are simply related to the number of molecules that was introduced in the start pulse and the dimensions of the simulation box.

When the molecules that initially are located in the rectangular start pulse are allowed to diffuse, they do so in such a way that equilibrium of the system is finally obtained. Therefore, the relative equilibrium concentrations of the system given in Fig. 11d also represent the propagator at $\Delta = \infty$, with $c_{\mathrm{wall}} = 0.1 \cdot c_{\mathrm{waterdomain}}$ and $c_{\mathrm{cell\ core}} = 0.5 \cdot c_{\mathrm{waterdomain}}$. Having established the initial and final states, we turn our focus to the diffusion process. At short time scales, most molecules diffuse freely, and as a result, Gaussian propagators are obtained. This is exemplified by the propagator of Fig. 11a, obtained after a diffusion time of 1 ms, where most molecules still reside inside the cell core. The molecules then reach the water domain where the concentration of labeled spins increases rapidly, as exemplified in Fig. 11b after a diffusion time of 10 ms. Essentially no molecules have entered the neighboring cells at this point, since the water diffusion out of each cell is restricted by the low water content in the cell walls. It is also evident that water diffuses out of the cell core against the water concentration gradient at this stage. The latter effect is still more pronounced when the

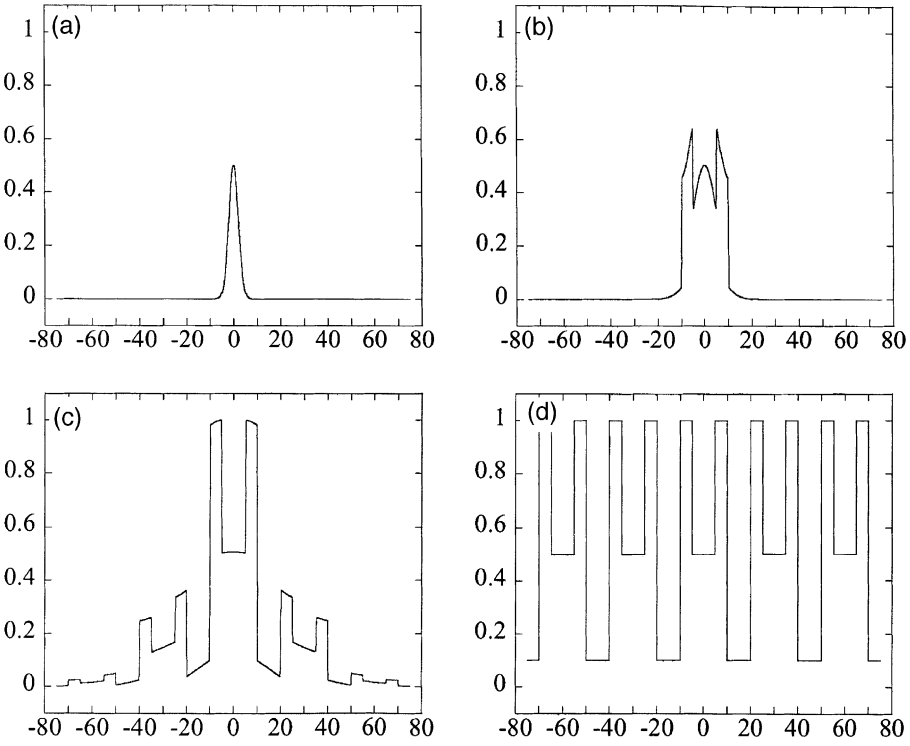

Fig. 11. The simulated propagators for the system described in Fig. 10 where the diffusion constant is $D = 2 \times 10^{-9}\,m^2\,s^{-1}$ in all three regions, from a centered starting pulse with a width of $\Delta z_{min} = 0.1\,\mu m$ after (a) 1 ms, (b) 10 ms, and (c) 0.3 s. In (d) the corresponding equilibrium concentration profile is given. The horizontal scales are in μm, and the concentrations on the vertical scales are given in relative units.

molecules leaves the cell wall and enter the water domain of a more distant unit cell, as shown in Fig. 11c at 0.3 s. At this stage, the cell core has an essentially homogenous water distribution, with a concentration that is half of that of the pure water domain.

The water molecules enter new cells, and in fact, the jagged propagators successively adopt an overall Gaussian shape, as is indicated already after diffusion for 0.3 s. For example, if only the concentration values obtained for the water domains are considered, a Gaussian curve may be reasonably well fitted, and the same is true if the concentration values of the cell walls or of the cell nucleuses are considered. The longer the diffusion time, the better the obtained fit.

However, sooner or later there will also be effects due to the finite size of the simulation box, and the propagators then exhibit increasing deviation from the Gaussian shape. Finally, as the time of propagation approaches infinity, equilibrium is obtained. As discussed above, Fig. 11d represent this state.

4. Future perspectives

The relationship between structure and dynamics of media that are porous on nano- and micro-scales is an area subject to intense research. In this context, NMR is a promising approach. It is our belief that the presented simulation methodology will be a useful tool in the analysis of experimental NMR data from porous systems.

We are presently extending the approach to the following areas.

(i) Simulations in 3-dimensions. This introduces no new concepts, but the calculations will be considerably more computer intensive.

(ii) Diffusion in the presence of external driving forces, such as pressure gradients, temperature gradients and gradients in chemical potential.

(iii) Generating echo-decay curves from an image of a porous system. This implies taking an image from a porous system, such as generated by e.g. confocal laser microscopy, and to simulate the propagator from the digitized image.

In principle, porous systems of any complexity can thus be studied. To generate a unique structure from an NMR diffusometry experiment is very difficult if additional information is not available. The opposite procedure is less demanding. We feel that the NMR diffusometry technique is perhaps best used to check structural data from other imaging techniques. Since the NMR approach is non-perturbing while many other imaging techniques are not, this is an important feature of the NMR diffusometry experiment.

Acknowledgments

The Swedish Agency for Innovation Systems, Vinnova, and the Swedish Research Council, VR, are gratefully acknowledged for financial support.

References

[1] P.T. Callaghan, Principles of Nuclear Magnetic Resonance Microscopy, Clarendon Press, Oxford, 1991.
[2] W.S. Price, Pulsed field gradient NMR as a tool for studying translational diffusion, Part 1. basic theory, Concepts Magn. Reson. 9 (1997) 299–336.
[3] W.S. Price, Pulsed-field gradient nuclear magnetic resonance as a tool for studying translational diffusion: Part II. experimental aspects, Concepts Magn. Reson. 10 (1998) 197–237.
[4] P.T. Callaghan, A. Coy, PGSE NMR and molecular translational motion in porous media, in: P. Tycko (Ed.), NMR Probes and Molecular Dynamics, Kluwer, Dordrecht, 1994, pp. 489–523.
[5] P.T. Callaghan, A. Coy, D. MacGowan, K.J. Packer, F.O. Zelaya, Diffraction-like effects in NMR diffusion of fluids in porous solids, Nature 351 (1991) 467–469.
[6] P.W. Küchel, A. Coy, P. Stilbs, NMR Diffusion-diffraction of water revealing alignment of erythrocytes in a magnetic field and their dimensions and membrane transport characteristics, Magn. Reson. Med. 37 (1997) 637–643.
[7] S.J. Gibbs, Observations of diffusive diffraction in a cylindrical pore by PFG NMR, J. Magn. Reson. 124 (1997) 223–226.
[8] B. Håkansson, O. Söderman, R. Pons, Structure determination of a highly concentrated W/O emulsion using PFG-SE NMR diffusion-diffractograms, Langmuir 15 (1998) 988–991.
[9] J. Kärger, W. Heink, The propagator representation of molecular transport in microporous crystallites, J. Magn. Reson. 51 (1983) 1–7.
[10] O. Söderman, P. Stilbs, NMR Studies of complex surfactant solutions, Prog. Nucl. Magn. Reson. Spectrosc. 26 (1994) 445–482.
[11] V.J. Wedeen, T.G. Reese, D.S. Tuch, M.R. Weigel, J.-G. Dou, R.M. Weiskoff, D. Chessler, Mapping fiber orientation in cerebral white matter with Fourier-transform diffusion MRI, Proc. Intl. Soc. Mag. Reson. Med. 8 (2000) 82.
[12] Y. Assaf, A. Mayk, Y. Cohen, Displacement imaging of spinal cord using *q*-space diffusion-weighted MRI, Magn. Reson. Med. 44 (2000) 713–722.
[13] P.T. Callaghan, A. Coy, T.P.J. Halpin, D. MacGowan, K.J. Packer, F.O. Zelaya, Diffusion in porous systems and the influence of pore morphology in pulsed field gradient spin-echo nuclear magnetic resonance studies, J. Chem. Phys. 97 (1992) 651–662.
[14] M.H. Blees, The effect of finite duration of gradient pulses on the pulsed-field-gradient NMR method for studying restricted diffusion, J. Magn. Reson. Ser. A 109 (1994) 203–209.
[15] P. Linse, O. Söderman, The validity of the short gradient pulse approximation in NMR studies of restricted diffusion. simulations of molecules diffusing between planes, in cylinders and spheres, J. Magn. Reson. Ser. A 116 (1995) 77–86.
[16] D.G. Regan, P.W. Küchel, Mean residence time of molecules diffusing in a cell bounded by a semi-permeable membrane: Monte Carlo simulations and an expression relating membrane transition probability to permeability, Eur. Biophys. J. Biophys. Lett. 29 (2000) 221–227.
[17] A.J. Lennon, P.W. Küchel, Neural networks used to interpret pulsed-gradient restricted-diffusion data, J. Magn. Reson. A 107 (1994) 229–235.
[18] P.W. Küchel, C.J. Durrant, Permeability coefficients from NMR *q*-space data: models with unevenly spaced semi-permeable parallel membranes, J. Magn. Reson. 139 (1999) 258–272.
[19] P.T. Callaghan, A simple matrix formalism for spin echo analysis of restricted diffusion under generalized gradient waveforms, J. Magn. Reson. 129 (1997) 74–84.
[20] A.V. Barzykin, Theory of spin echo in restricted geometries under a step-wise gradient pulse sequence, J. Magn. Reson. 139 (1999) 342–353.
[21] J.E. Tanner, E.O. Stejskal, Restricted self-diffusion of protons in colloidal systems by the pulsed-gradient, spin-echo method, J. Chem. Phys. 49 (1968) 1768–1777.
[22] J.E.M. Snaar, H. van As, NMR self-diffusion measurements in a bounded system with loss of magnetization at the walls, J. Magn. Reson. Ser. A 102 (1993) 318–326.
[23] B. Jönsson, H. Wennerström, P.G. Nilsson, P. Linse, Self-diffusion of small molecules in colloidal systems, Colloid Polym. Sci. 264 (1986) 77–88.
[24] http://www.comsol.com.
[25] http://www.mathworks.com.
[26] W.H. Press, Numerical Recipes, Cambridge University Press, Cambridge, MA, 1990.